CCIT Report #386
May 2002

Detection and Extraction of Fault Surfaces in 3-D Seismic Data

Israel Cohen*

Department of Electrical Engineering
Technion - Israel Institute of Technology
Technion City, Haifa 32000, Israel

Abstract

In this paper, an efficient method is proposed for detecting and extracting fault surfaces in 3-D seismic volumes. The seismic data is transformed into a volume of Local Fault Extraction (LFE) estimates, representing the likelihood that a given point lies on a fault surface. The fault surfaces are partitioned into relatively small linear portions, which are identified by analyzing tilted and rotated subvolumes throughout the region of interest. Directional filtering and thresholding further enhance the seismic discontinuities attributable to fault surfaces. The LFE method demonstrates a more reliable and convenient interpretation tool for fault surfaces, compared to the state-of-the-art coherence analysis. In particular subtle faults having minimal offsets can be detected in noisy complex geological structures.

*E-mail: icohen@ee.technion.ac.il; Tel.: +972 4 8294731; Fax: +972 4 8323041

Introduction

Fault surfaces are common subterranean structures, associated with displacements or offsets of seismic layers. Their consistent and reliable detection in 3-D seismic data provides an interpreter with very powerful means to quickly visualize and map complex geological structures.

A common tool facilitating structural and stratigraphic interpretation is the coherency cube, originated by Bahorich and Farmer (1995, 1996). It is calculated from the seismic data using a coherency measure that quantifies the seismic discontinuity at each point. Discontinuities attributable to fault surfaces include dip, azimuth, and offset changes of seismic reflectors, and waveform and amplitude variations caused by defocusing. Such discontinuities appear on coherence slices as incoherent linear or curved features (*e.g.*, Marfurt *et al.* 1999; Gersztenkorn *et al.* 1999; Neff *et al.* 2000; Lees 1999).

The most acceptable coherence measures are based on cross correlation (Bahorich and Farmer 1995), semblance (Marfurt *et al.* 1998), or eigenstructure (Gersztenkorn and Marfurt 1996a, 1996b; Kirlin 1992) techniques. These methods typically suffer from either a lack of robustness, especially when dealing with noisy data, or high computational complexity (Marfurt *et al.* 1999; Gersztenkorn and Marfurt 1999). Recently, we have introduced a multiscale analysis method for the estimation of seismic coherency, which is both robust to noise and computationally efficient (Cohen and Coifman 2001). It involves a coherency measure, namely the *Local Structural Entropy* (LSE), which evaluates the dissimilarity of subvolumes enclosing a given analysis point. Dealing with subvolumes, rather than individual traces, leads to robustness, while avoiding the expensive computations of semblance and eigenstructure-based large covariance matrices and eigenvalues.

A major drawback of coherency-based fault analysis is that seismic discontinuities may also result from geological features, which are unrelated to faults. Furthermore, creating a consistent geological interpretation from large 3-D seismic data volumes often requires manual intervention,

which is time-consuming, tedious and imprecise.

In this paper, we propose a robust and computationally efficient method for the extraction of fault surfaces in 3-D seismic volumes. The seismic data is transformed into a volume of Local Fault Extraction (LFE) estimates, which provides the interpreter with a much clearer visual indication of the fault surfaces. The LFE estimate at a given analysis point is obtained by the following procedure. First, a 3-D analysis cube, tilted and rotated about the analysis point, is selected by the interpreter. The analysis cube moves throughout the seismic volume and outputs for each point a measure of Normalized Differential Entropy (NDE). The NDE value represents the likelihood of a fault surface, having similar dip and azimuth as of the analysis cube, to intersect with the analysis point. Subsequently, the local average of the NDE is removed, and portions of fault surfaces, approximately aligned with the analysis cube, are extracted by directional filtering. The filtered NDE coefficients are thresholded, and filtered back to produce directional LFE volumes. Finally, the LFE attribute is given by the maximal directional LFE, over the presumably tested set of dips and azimuths. This practically gathers the significant portions of the fault surfaces into smooth larger surfaces. A comparison of the LFE volume with the state of the art coherence volumes shows that the LFE method provides a more reliable and convenient tool for detecting and extracting fault surfaces, in particular subtle faults in complex geological structures.

The Local Fault Extraction

In this section we describe the basic components forming the proposed fault extraction algorithm.

Normalized Differential Entropy

We begin by subtracting the mean value from each trace of the seismic data . Specifically, the data is modified by

$$\hat{d}_{xyt} = d_{xyt} - E_t\{d_{xyt}\} = d_{xyt} - \tfrac{1}{N_t}\sum_{k=1}^{N_t} d_{xyk}\,, \tag{1}$$

where d_{xyt} and $\hat{d}_{xyt}$ are respectively the original and modified t-th sample of the trace at position (x, y), and N_t is the total number of samples in each trace. Then, a relatively small 3-D analysis cube is selected by the interpreter. The analysis cube moves throughout the 3-D modified seismic volume and outputs for each point a measure of NDE.

The analysis cube is defined by the length of major axis L_1, length of minor axis $2L_2 + 1$, time duration N samples, azimuth φ, and dip γ (Fig. 1). It comprises two identical subvolumes, which are tilted and rotated about the analysis point $\lambda = (x, y, t)$. The samples within the two subvolumes are rearranged in a consistent manner into two column vectors $\mathbf{v}_{1,\lambda}(\gamma, \varphi)$ and $\mathbf{v}_{2,\lambda}(\gamma, \varphi)$. The NDE at the analysis point λ is defined by the normalized difference of this two vectors:

$$\mathcal{N}_\lambda(\gamma, \varphi) = \frac{\|\mathbf{v}_{1,\lambda}(\gamma, \varphi) - \mathbf{v}_{2,\lambda}(\gamma, \varphi)\|_p}{\|\mathbf{v}_{1,\lambda}(\gamma, \varphi)\|_p + \|\mathbf{v}_{2,\lambda}(\gamma, \varphi)\|_p}\,, \tag{2}$$

where $\|\cdot\|_p$ is the ℓ_p norm. The NDE is a gradient based formula and is a normalized version of the Prewitt edge detection filter (Jain, 1989), (Lipkin and Rosenfeld,1970). In order words the NDE computations are an extension of edge detection to surface detection in three dimensions. If the two subvolumes are perfectly correlated without a disruption or offset of seismic layers, presumably there is not fault surface enclosed between them, so $\mathbf{v}_{1,\lambda}(\gamma, \varphi) = \mathbf{v}_{2,\lambda}(\gamma, \varphi)$ and $\mathcal{N}_\lambda(\gamma, \varphi) = 0$. Otherwise, the likelihood for the presence of a fault surface, aligned in the gap between the two subvolumes, is proportional to the offset of $\mathbf{v}_{1,\lambda}(\gamma, \varphi)$ and $\mathbf{v}_{2,\lambda}(\gamma, \varphi)$. In this case, $0 < \mathcal{N}_\lambda(\gamma, \varphi) \leq 1$, where the maximum value of $\mathcal{N}_\lambda(\gamma, \varphi)$ is obtained for maximally offset correlated subvolumes, *i.e.*,

$\mathbf{v}_{1,\lambda}(\gamma,\varphi) = -\mathbf{v}_{2,\lambda}(\gamma,\varphi)$.

Contrast Enhancement

The second step of the algorithm is contrast enhancement. Fault surfaces having dips and azimuths about the same dip and azimuth of the analysis cube are distinguished by higher NDE values, compared to the local average NDE value. Accordingly, we apply a contrast enhancement filtering to the NDE values, and set to zero negative values. This facilitates the analysis of regions that contain dipping layers or are highly discontinuous.

The contrast enhancement filtering can be efficiently implemented using a discrete "Mexican Hat" function:

$$f(n) = C(1-n^2)\exp(-n^2/2) \tag{3}$$

where $n = k\tau$ ($k \in \mathbb{Z}$), C is a normalization constant such that $\sum_{k=-\infty}^{\infty} |f(k\tau)| = 2$. We use a finite length filter ($-4.5 \leq n \leq 4.5$), containing odd number of uniformly spaced coefficients (we obtained good results for 31 coefficients, but generally it depends on the size of the analysis cube and the "thickness" of the fault surfaces). The filtered NDE is given by:

$$\bar{\mathcal{N}}_\lambda(\gamma,\varphi) = g_\lambda(\gamma,\varphi) * \mathcal{N}_\lambda(\gamma,\varphi) = \sum_{\lambda'} g_{\lambda-\lambda'}(\gamma,\varphi)\mathcal{N}_{\lambda'}(\gamma,\varphi)\,, \tag{4}$$

where $g_\lambda(\gamma,\varphi)$ is a rotated version of f, such that its main axis is perpendicular to the slabs of the analysis cube. The contrast enhanced NDE is given by

$$\hat{\mathcal{N}}_\lambda(\gamma,\varphi) = \max\left\{\bar{\mathcal{N}}_\lambda(\gamma,\varphi),\, 0\right\}\,. \tag{5}$$

Directional LFE

The third step of the algorithm is directional filtering. In this step, we extract the portions of fault surfaces that are approximately aligned with the analysis cube.

The directional filter, denoted by $h_\lambda(\gamma+\alpha,\varphi)$, is a 3-D ellipsoid, tilted by $\gamma+\alpha$ with respect to the time axis, rotated by φ with respect to the in-line axis, and normalized by $\sum_\lambda h_\lambda(\gamma,\varphi) = 1$. Its dimensions, selected by the interpreter, control the minimal dimensions of the detected subsurfaces. The maximum value of α is determined by the dip increment Δ_γ ($|\alpha| < \Delta_\gamma/2$). In our implementation, we used a 3-D pencil-like shaped Hanning window, whose dimensions are 61 samples at its major axis and 3 samples at its minor axes. The dip increment is $\Delta_\gamma = 5^o$, and the relative tilt of the directional filter α is restricted to $\{-2^o, 0, 2^o\}$. Clearly, we could use a smaller dip increment and discard the relative tilt. However, the above formulation is computationally more efficient.

Directional filtering of the contrast enhanced NDE yields

$$C_\lambda(\gamma+\alpha,\varphi) = \sum_{\lambda'} h_{\lambda-\lambda'}(\gamma+\alpha,\varphi)\hat{\mathcal{N}}_{\lambda'}(\gamma,\varphi)\,. \tag{6}$$

These coefficients are thresholded by δ ($0 < \delta < 1$),

$$\tilde{C}_{\lambda'}(\gamma+\alpha,\varphi) = \begin{cases} C_{\lambda'}(\gamma+\alpha,\varphi), & \text{if } C_{\lambda'}(\gamma+\alpha,\varphi) \geq \delta \\ 0, & \text{otherwise,} \end{cases} \tag{7}$$

and then filtered back to produce the directional LFE, given by

$$\mathcal{L}_\lambda(\gamma,\varphi) = \sum_{\lambda',\alpha} \tilde{C}_{\lambda'}(\gamma+\alpha,\varphi) h_{\lambda-\lambda'}(\gamma+\alpha,\varphi)\,. \tag{8}$$

The directional LFE volumes contain significant portions of fault surfaces, characterized by roughly the same dip and azimuth orientations as those of the analysis cube.

Constructing the Fault Surfaces

The final step of the algorithm is keeping at each point the maximum directional LFE value, over the tested set of dips and azimuths. Specifically, the LFE attribute at the analysis point λ is given by

$$\mathcal{L}_\lambda = \max_{\gamma,\varphi} \{\mathcal{L}_\lambda(\gamma,\varphi)\} \ . \tag{9}$$

The LFE volume thus gathers and connects the significant portions of faults into smooth large fault surfaces.

Results

In this section we use a real data example to demonstrate the applicability of the LFE algorithm, and to illustrate its execution. The data example (courtesy of GeoEnergy) is from the Gulf of Mexico. The data is decimated in both time and space. The time interval is $8\,ms$, in-line trace spacing is $25\,m$, and cross-line trace spacing is $50\,m$. A small subvolume with an in-line distance of $5.025\,km$ and a cross-line distance of $10.05\,km$ (201 x 201 traces) is used for demonstration. Each trace is $3.208\,s$ in duration (401 samples).

Fig. 2 shows a vertical cross-section through the seismic data at $y = 6\,km$. The corresponding cross-sections through the NDE volumes, obtained with an analysis cube of [7 7 21] samples and various dips and azimuths, are displayed in Fig. 3. Clearly, the dip and azimuth of the analysis cube determine the portions of fault surfaces to be detected. In particular, surfaces having dips and azimuths about the same dip and azimuth of the analysis cube are distinguished by higher NDE values, compared to the locally averaged NDE. The second step of the algorithm is contrast enhancement. This step removes the 3-D local average of the NDE, thus compensating for regions that are highly discontinuous, but often do not contain fault surfaces. The results of the second

step are displayed in Fig. 4. The third step of the algorithm is directional filtering. Here, we detect the portions of fault surfaces that are approximately aligned with the analysis cube. The minimal dimensions of the detected subsurfaces are controlled by the dimensions of the directional filter. For the present example, we used a 3-D pencil-like shaped Hanning filter, whose dimensions are 61 samples at its major axis and 3 samples at its minor axes. The dip increment is $\Delta_\gamma = 5^o$, the azimuth increment is $\Delta_\varphi = 45^o$, and the relative tilt of the directional filter α is restricted to $\{-2^o, 0, 2^o\}$. The filtered NDE coefficients are thresholded by $\delta = 0.12$, and filtered back to produce the directional LFE volumes. The results of the third step of the algorithm are displayed in Fig. 5. The final step is keeping at each point the maximum value. This yields the LFE volume (Fig. 6), containing all the fault surfaces in conformity with the presumed model (*i.e.*, the dimensions of the analysis cube, set of dips and azimuths, directional filter, threshold, *etc.*).

For comparison with the state of the art coherence attributes, we plot in Fig. 7 the vertical cross-sections at $y = 6\,km$ through the LSE (Cohen and Coifman 2001) and the eigenstructure-based coherence volumes (Gersztenkorn and Marfurt 1999), using an analysis cube of [6 6 21] samples. Values are mapped to shades of gray, where darker shades indicate greater discontinuity. These methods produce similar images. However, the LSE-based algorithm is computationally much more efficient than the eigenstructure-based algorithm (Cohen and Coifman 2001). A comparison of Figs. 6 and 7 shows that the LFE method provides a more reliable and convenient tool for the extraction of subtle fault surfaces. This is further shown in Fig. 8, which compares the horizontal slices at $t = 480ms$ through the LFE, the LSE, and the eigenstructure-based coherence volumes.

Acknowledgements

The author would like to thank Prof. Ronald R. Coifman of Yale University and Dr. Anthony Vassiliou of GeoEnergy for valuable discussions and helpful suggestions.

References

Bahorich, M. S., and Farmer, S. L., 1995, 3-D seismic discontinuity for faults and stratigraphic features: The Leading Edge, **14**, 1053–1058.

Bahorich, M. S., and Farmer, S. L., 1996, Methods of seismic signal processing and exploration: US Patent 5 563 949.

Cohen, I., and Coifman, R. R., 2001, Multiscale Local Discontinuity Measures for 3-D Seismic Data: Submitted to Geophysics.

Gersztenkorn, A., and Marfurt, K. J., 1996a, Coherence computations with eigenstructure: 58th Conf. and Tech. Exhibition, Eur. Assn. Geosci. Eng., Extended Abstracts, X031.

Gersztenkorn, A., and Marfurt, K. J., 1996b, Eigenstructure based coherence computations: 66th Ann. Internat. Mtg., Soc. Expl. Geophys., Extended Abstracts, 328–331.

Gersztenkorn, A., and Marfurt, K. J., 1999, Eigenstructure-based coherence computations as an aid to 3-D structural and stratigraphic mapping: Geophysics, **64**, 1468–1479.

Gersztenkorn, A., Sharp, J., and Marfurt, K. J., 1999, Delineation of tectonic features offshore Trinidad using 3-D seismic coherence: The Leading Edge, **18**, 1000–1008.

Kirlin, R. L., 1992, The relationship between semblance and eigenstructure velocity estimators: Geophysics, **57**, 1027–1033.

Lees, J. A., 1999, Constructing faults from seed picks by voxel tracking: The Leading Edge, 338–340.

Marfurt, K. J, Kirlin, R. L., Farmer, S. L., and Bahorich, M. S., 1998, 3-D seismic attributes using a semblance-based coherency algorithm: Geophysics, **63**, 1150–1165.

Marfurt, K. J, Sudhaker, V., Gersztenkorn, A., Crawford, K. D., and Nissen, S. E., 1999, Coherency calculations in the presence of structural dip: Geophysics, **64**, 104–111.

Jain, A. K, Fundamentals of Digital Image Processing, Prentice Hall Information and System Science Series, Thomas Kailath Editor, 1989.

Lipkin, B. S, Rosenfiled, A. (eds.). Picture Processing and Psychopictorics. New York. Academic Press, 1970.

Neff, D. B., Grismore, J. R., and Lucas, W. A., 2000, Automated seismic fault detection and picking: US Patent 6 018 498.

Figure Captions

Fig. 1: (a) A vertical cross-section and (b) horizontal slice illustrating the geometrical distribution of traces and samples used in the analysis cube. The analysis cube, consisting of two subvolumes, is centered about an analysis point $\lambda = (x, y, t)$, and defined by length of major axis L_1, length of minor axis $2L_2 + 1$, time duration N samples, azimuth φ, and dip γ.

Fig. 2: A vertical cross-section through the seismic data at $y = 6\,km$.

Fig. 3: First step of the algorithm: Computing the Normalized Differential Entropy. Vertical cross-sections at $y = 6\,km$ through NDE volumes, using an analysis cube of [7 7 21] samples and the following dips and azimuths: (a) $\gamma = -20^o$, $\varphi = 0^o$. (b) $\gamma = -5^o$, $\varphi = 0^o$. (c) $\gamma = 0^o$, $\varphi = -45^o$. (d) $\gamma = 0^o$, $\varphi = 0^o$. (e) $\gamma = 5^o$, $\varphi = 0^o$. (f) $\gamma = 15^o$, $\varphi = 20^o$.

Fig. 4: Second step of the algorithm: Contrast enhancement. Vertical cross-sections at $y = 6\,km$ through contrast enhanced NDE volumes, using an analysis cube of [7 7 21] samples and the following dips and azimuths: (a) $\gamma = -20^o$, $\varphi = 0^o$. (b) $\gamma = -5^o$, $\varphi = 0^o$. (c) $\gamma = 0^o$, $\varphi = -45^o$. (d) $\gamma = 0^o$, $\varphi = 0^o$. (e) $\gamma = 5^o$, $\varphi = 0^o$. (f) $\gamma = 15^o$, $\varphi = 20^o$.

Fig. 5: Third step of the algorithm: Directional filtering. Vertical cross-sections at $y = 6\,km$ through directional LFE volumes, using an analysis cube of [7 7 21] samples and the following dips and azimuths: (a) $\gamma = -20^o$, $\varphi = 0^o$. (b) $\gamma = -5^o$, $\varphi = 0^o$. (c) $\gamma = 0^o$, $\varphi = -45^o$. (d) $\gamma = 0^o$, $\varphi = 0^o$. (e) $\gamma = 5^o$, $\varphi = 0^o$. (f) $\gamma = 15^o$, $\varphi = 20^o$.

Fig. 6: Final step of the algorithm: Maximizing over a set of dips and azimuths. A vertical cross-section at $y = 6\,km$ through the LFE volume, using an analysis cube of [7 7 21] samples, dips $\gamma = -20^o, -15^o, \ldots, 20^o$, and azimuths $\varphi = -45^o, 0^o, 45^o, 90^o$.

Fig. 7: Vertical cross-sections at $y = 6\,km$ through (a) the Local Structural Entropy volume, and

(b) the eigenstructure-based coherence volume, using an analysis cube of [6 6 21] samples.

Fig. 8: Horizontal slices at $t = 480ms$ through (a) the seismic data, (b) the eigenstructure-based coherence volume using an analysis cube of [6 6 21] samples, (c) the LSE volume using an analysis cube of [6 6 21] samples, and (d) the LFE volume using an analysis cube of [7 7 21] samples.

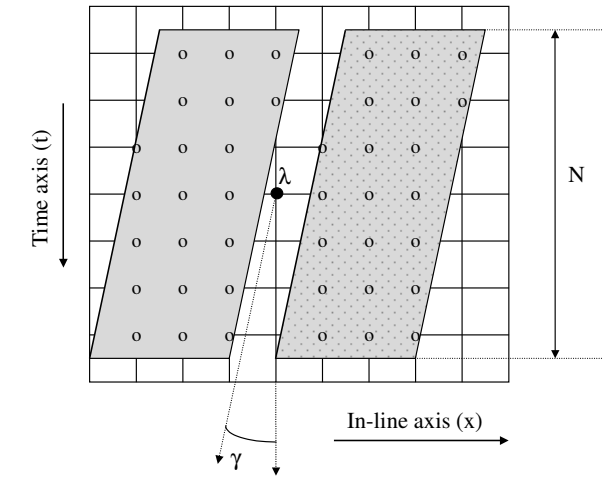

(a)

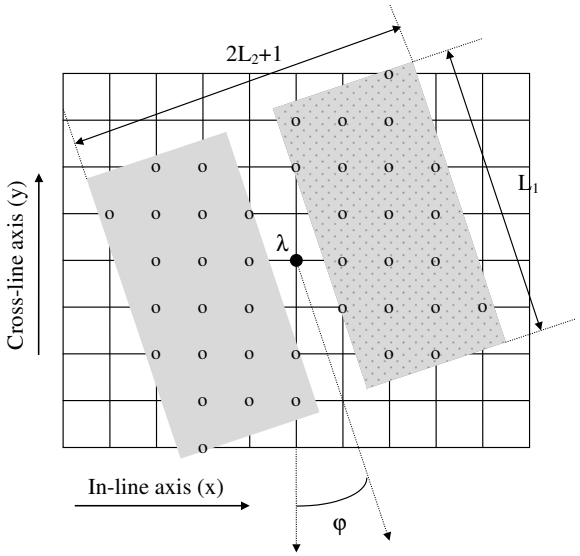

(b)

Figure 1: (a) A vertical cross-section and (b) horizontal slice illustrating the geometrical distribution of traces and samples used in the analysis cube. The analysis cube, consisting of two subvolumes, is centered about an analysis point $\lambda = (x, y, t)$, and defined by length of major axis L_1, length of minor axis $2L_2 + 1$, time duration N samples, azimuth φ, and dip γ.

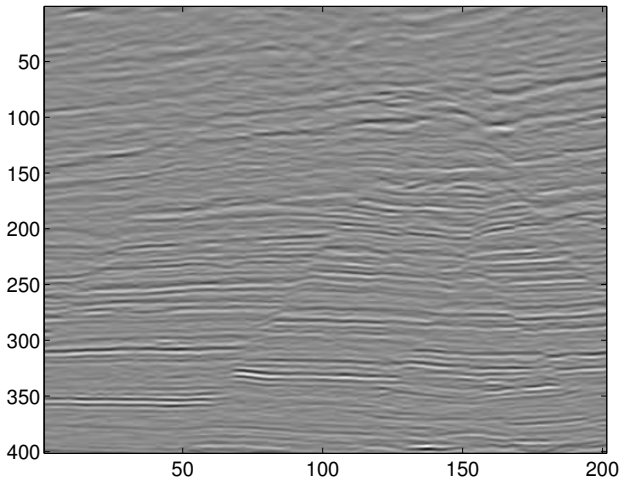

Figure 2: A vertical cross-section through the seismic data at $y = 6\,km$.

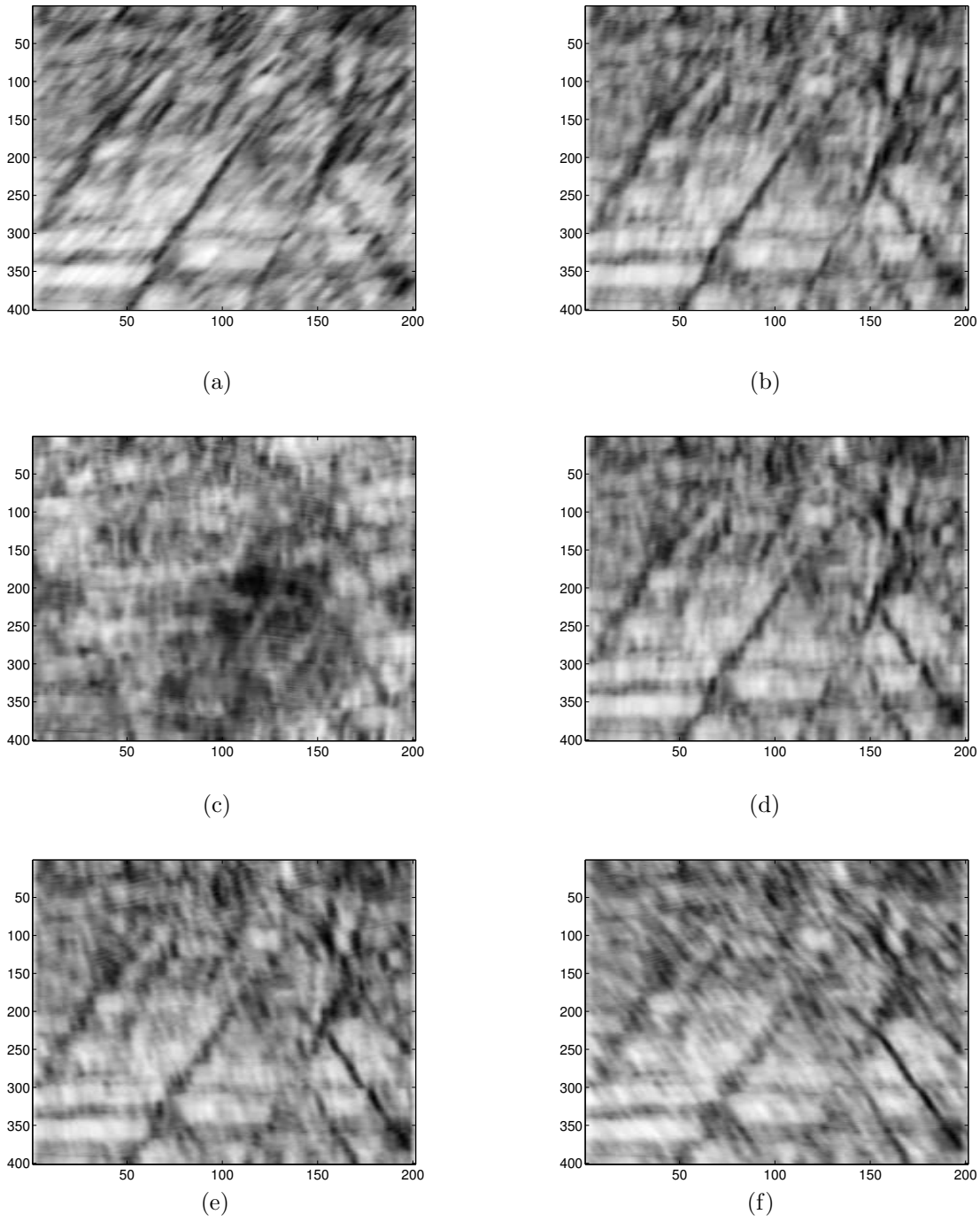

(a) (b)

(c) (d)

(e) (f)

Figure 3: First step of the algorithm: Computing the Normalized Differential Entropy. Vertical cross-sections at $y = 6\,km$ through NDE volumes, using an analysis cube of [7 7 21] samples and the following dips and azimuths: (a) $\gamma = -20^o$, $\varphi = 0^o$. (b) $\gamma = -5^o$, $\varphi = 0^o$. (c) $\gamma = 0^o$, $\varphi = -45^o$. (d) $\gamma = 0^o$, $\varphi = 0^o$. (e) $\gamma = 5^o$, $\varphi = 0^o$. (f) $\gamma = 15^o$, $\varphi = 20^o$.

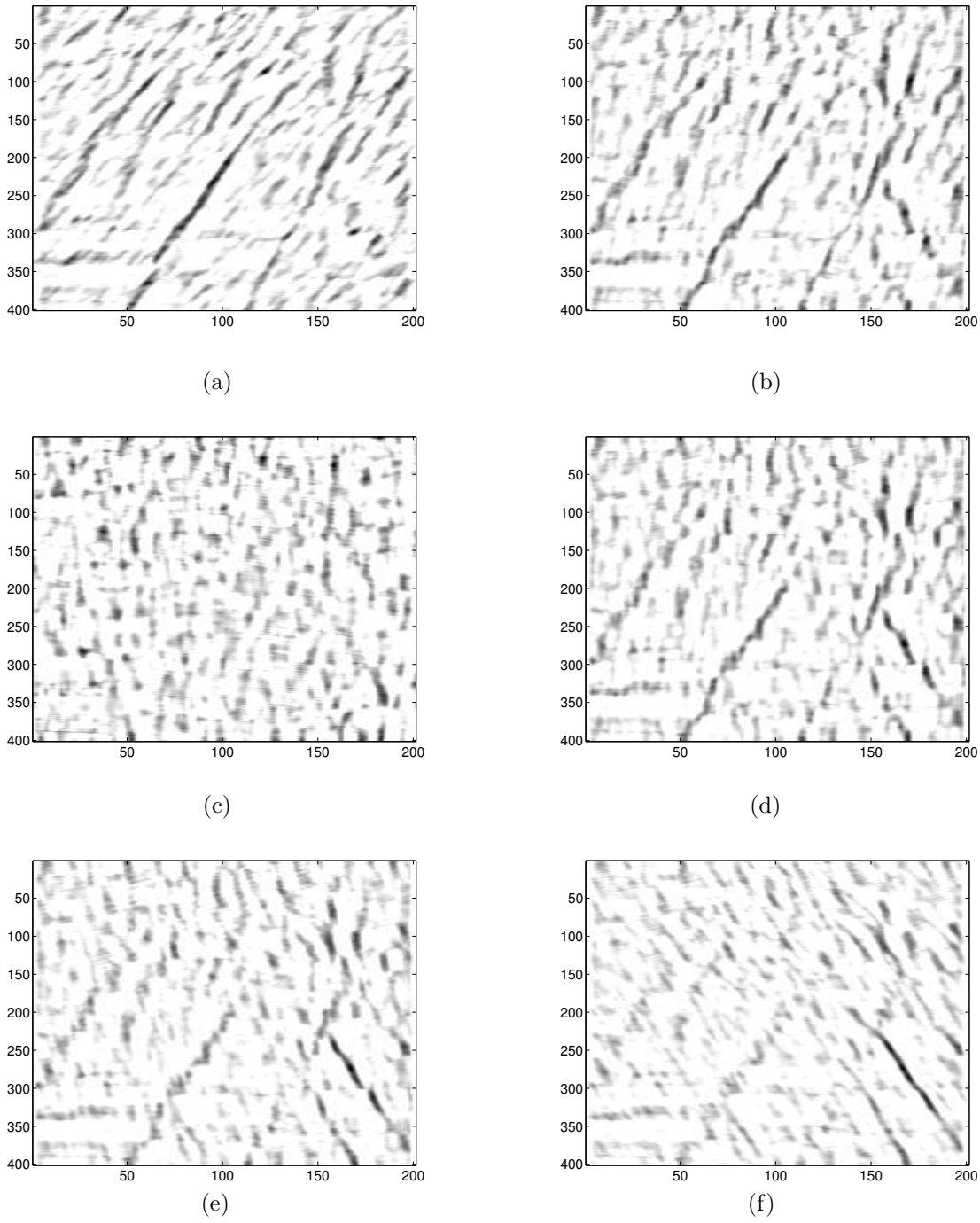

Figure 4: Second step of the algorithm: Contrast enhancement. Vertical cross-sections at $y = 6\,km$ through contrast enhanced NDE volumes, using an analysis cube of [7 7 21] samples and the following dips and azimuths: (a) $\gamma = -20^o$, $\varphi = 0^o$. (b) $\gamma = -5^o$, $\varphi = 0^o$. (c) $\gamma = 0^o$, $\varphi = -45^o$. (d) $\gamma = 0^o$, $\varphi = 0^o$. (e) $\gamma = 5^o$, $\varphi = 0^o$. (f) $\gamma = 15^o$, $\varphi = 20^o$.

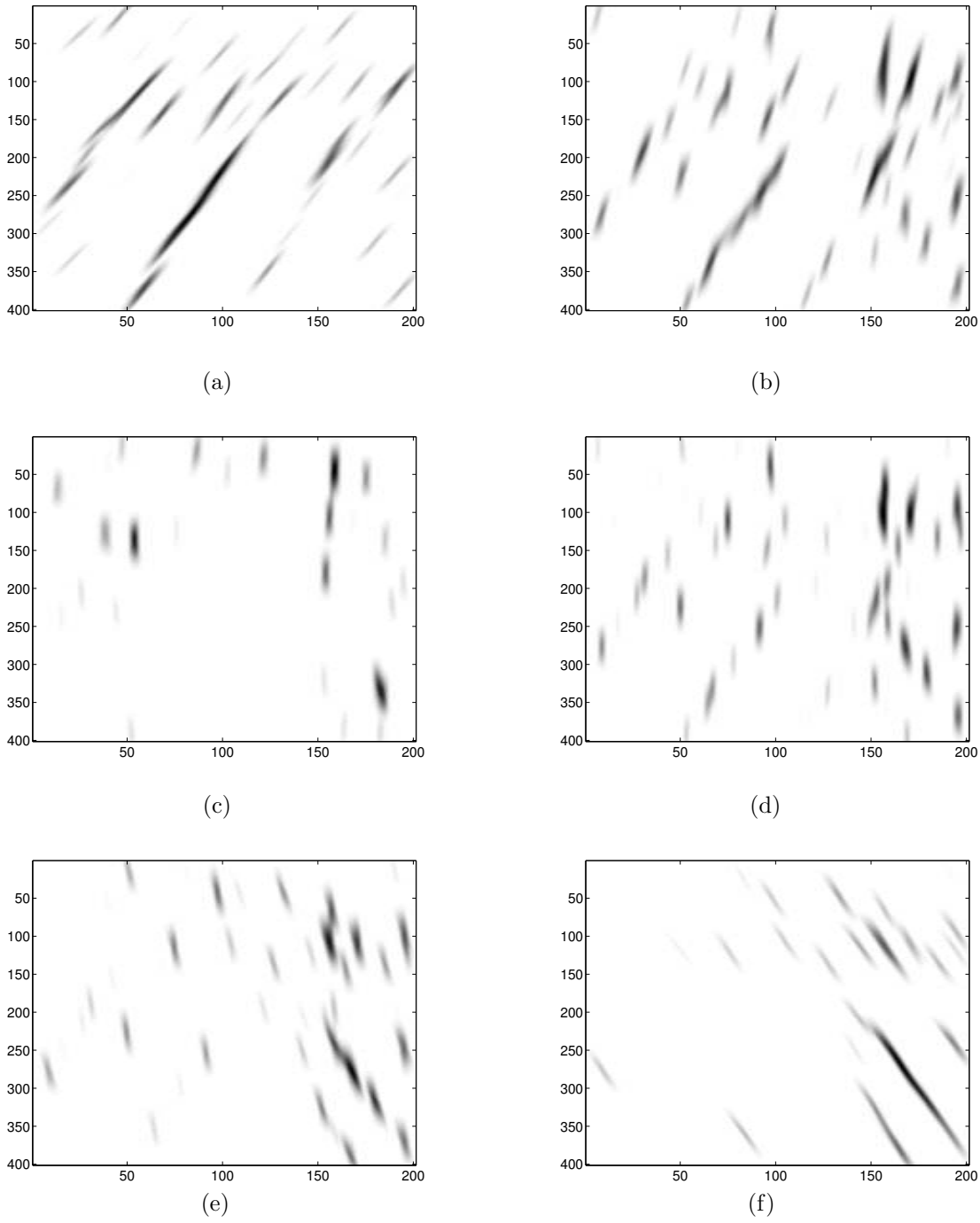

(a) (b)

(c) (d)

(e) (f)

Figure 5: Third step of the algorithm: Directional filtering. Vertical cross-sections at $y = 6\,km$ through directional LFE volumes, using an analysis cube of [7 7 21] samples and the following dips and azimuths: (a) $\gamma = -20^o$, $\varphi = 0^o$. (b) $\gamma = -5^o$, $\varphi = 0^o$. (c) $\gamma = 0^o$, $\varphi = -45^o$. (d) $\gamma = 0^o$, $\varphi = 0^o$. (e) $\gamma = 5^o$, $\varphi = 0^o$. (f) $\gamma = 15^o$, $\varphi = 20^o$.

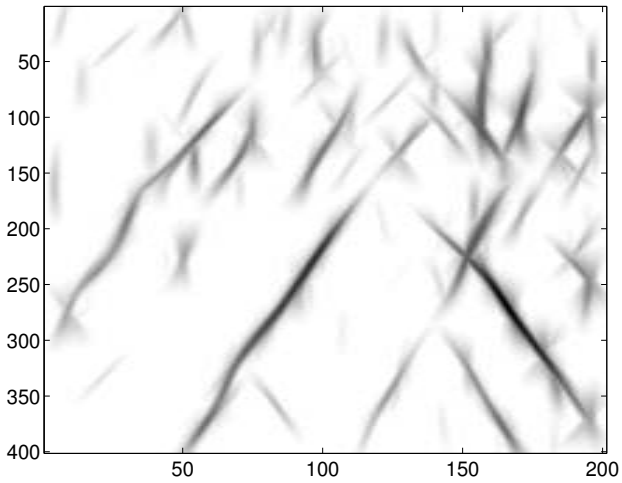

Figure 6: Final step of the algorithm: Maximizing over a set of dips and azimuths. A vertical cross-section at $y = 6\,km$ through the LFE volume, using an analysis cube of [7 7 21] samples, dips $\gamma = -20^o, -15^o, \ldots, 20^o$, and azimuths $\varphi = -45^o, 0^o, 45^o, 90^o$.

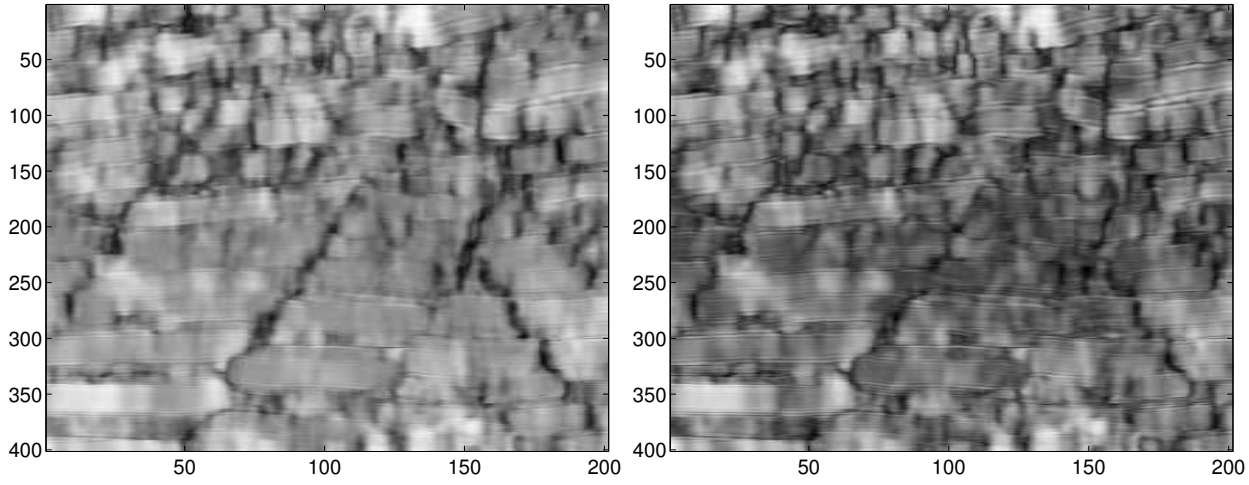

(a) (b)

Figure 7: Vertical cross-sections at $y = 6\,km$ through (a) the Local Structural Entropy volume, and (b) the eigenstructure-based coherence volume, using an analysis cube of [6 6 21] samples.

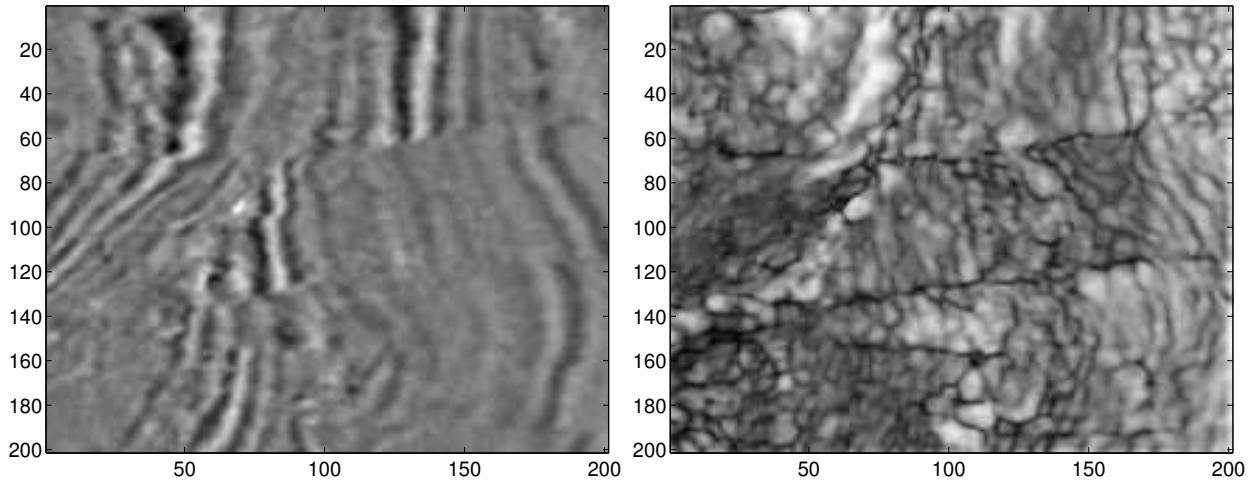

(a) (b)

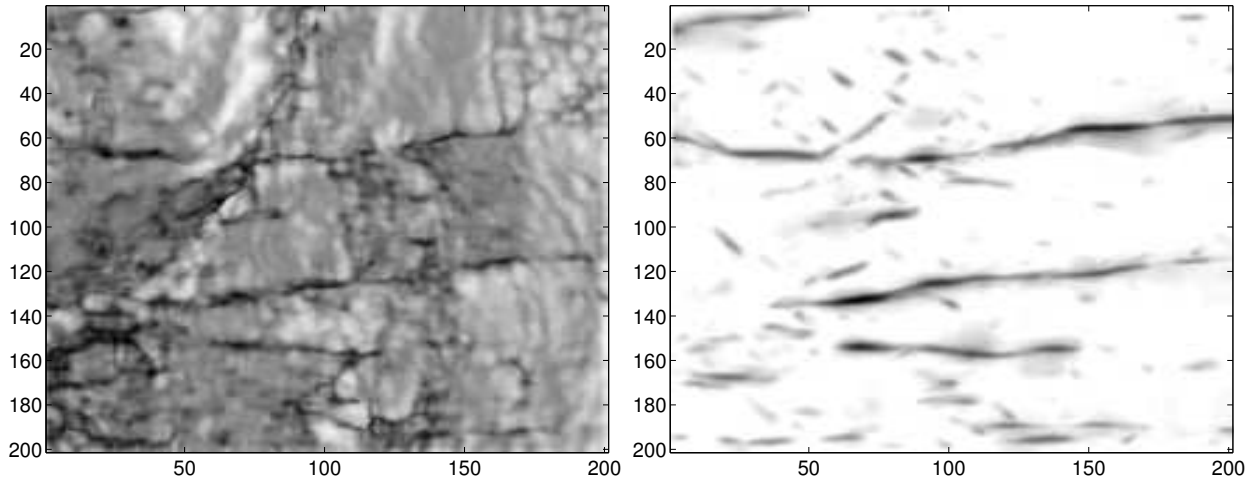

(c) (d)

Figure 8: Horizontal slices at $t = 480ms$ through (a) the seismic data, (b) the eigenstructure-based coherence volume using an analysis cube of [6 6 21] samples, (c) the LSE volume using an analysis cube of [6 6 21] samples, and (d) the LFE volume using an analysis cube of [7 7 21] samples.